3-2-2022

The Arecibo Observatory as an Instrument for Investigating Orbital Debris: Legacy and Next Generation Performance

James Murray
The University of Texas Rio Grande Valley

Fredrick A. Jenet
Expanding Frontiers

Recommended Citation

James Murray and Fredrick Jenet 2022 Planet. Sci. J. 3 52. https://doi.org/10.3847/PSJ/ac4d96

The Planetary Science Journal, 3:52 (12pp), 2022 March https://doi.org/10.3847/PSJ/ac4d96

The Arecibo Observatory as an Instrument for Investigating Orbital Debris: Legacy and Next Generation Performance

James Murray[1,2] and Fredrick Jenet[3]
[1] Center for Advanced Radio Astronomy, University of Texas Rio Grande Valley, One West University Boulevard, Brownsville, TX 78520, USA
[2] University of Texas at Arlington, 701 South Nedderman Drive, Arlington, TX 76019, USA
[3] Expanding Frontiers, 495 Amelia Earhart Drive, Suite A, Brownsville, TX 78521, USA
Received 2021 September 7; revised 2021 December 8; accepted 2022 January 19; published 2022 March 2

Abstract

In this paper, we investigate the ability of the Arecibo Observatory to characterize the orbital debris environment and compare it to the primary instrument used by NASA's Orbital Debris Program Office, the Haystack Ultra-Wideband Satellite Imaging Radar (HUSIR). Arecibo's location (18°.3 N) increases the percentage of observable orbits (relative to HUSIR) by 27%, which gives Arecibo access to a much larger and previously unmeasured portion of the environment. Due to the recent collapse of the Arecibo dish, in addition to exploring historic capabilities of the Legacy Arecibo Telescope, estimates of the performance of the proposed Next Generation Arecibo Telescope (NGAT) are explored. We show that the current NGAT design could have a sensitivity comparable to the Goldstone Orbital Debris Radar, currently NASA's most sensitive orbital debris radar. Additionally, design suggestions are presented that would significantly improve the capabilities of the NGAT for orbital debris investigations. We show that, with appropriate hardware upgrades, it would be possible to achieve a minimum-detectable debris size as small as 1 mm. These capabilities would allow data from Arecibo to significantly improve short-term debris environment models, which are used to inform spacecraft design and operations, particularly for orbital debris smaller than 3 mm, which pose the highest penetration risk to most spacecraft.

Unified Astronomy Thesaurus concepts: Space debris (1542); Radar telescopes (1330)

1. Introduction

Orbital debris are all man-made objects in orbit about the Earth that no longer serve a useful purpose. There are currently more than 23,000 tracked objects greater than 10 cm in diameter, approximately 500,000 objects between 1 and 10 cm, and over 100 million objects less than 1 cm (Liou 2020). Debris as small as 0.1 mm can penetrate a space suit, 1 mm debris could damage the space shuttle payload bay, and 5 mm debris could penetrate the space shuttle crew cabin (National Research Council et al. 1998). The nominal size limit for debris that is tracked and can be avoided is 10 cm. Debris smaller than this, while still dangerous, cannot be avoided. The risk they pose must be mitigated through advanced shielding techniques. This makes understanding the small debris environment in low Earth orbit (LEO) crucial for spacecraft design and operation. For many years, NASA has developed statistical engineering models of the orbital debris environment to inform spacecraft operators and designers of the potential hazards posed by debris and allow them to minimize the risk to satellites and spacecraft that can result in significant monetary loss and potentially loss of life.

NASA's Orbital Debris Program Office (ODPO) gathers their data for objects greater than 10 cm from the United States Space Surveillance Network (SSN). For objects smaller than approximately 1 mm, data comes from in-situ measurements analyzing the impact craters from returned spacecraft. Terrestrial radar fills in the gap between the in-situ measurements and the two-line element-derived SSN data, where HUSIR has a size limit of 5.5 mm (Stansbery et al. 2014) at 1000 km. This leaves a small area between approximately 1 mm and 1 cm for which there is little data available in LEO.

The SSN consists of sensors, both radar and optical, that are located all around the world. The distribution of sensors is such that orbits of any inclination can be measured. The HUSIR radar is located at 42°.6 N latitude. Since the normal observation mode involves staring east at 75° elevation (Murray et al. 2019a), the minimum orbital inclination that can be measured at full sensitivity in the 5 mm to 1 cm range is approximately 42°. Observation modes involving staring south at low-elevation angles give HUSIR access to lower inclinations, but at the cost of reduced sensitivity due to increased slant ranges. The Goldstone Orbital Debris Radar system, located at 35°.4 N, is also used as a collateral sensor, but is limited in both observable orbital inclinations and available observation time (Murray et al. 2019b).

In 2015, NASA published the Micrometeoroid and Orbital Debris Assessment of the Joint Polar Satellite System (Squire et al. 2015). A key finding of the report states that the greatest risk to spacecraft is posed by orbital debris in the 0.6 to 3 mm size regime. Additionally, the report compared the predicted debris flux using several orbital debris environment models including NASA's Orbital Debris Engineering Model (ORDEM) 3.0, NASA's ORDEM 2000 (an older version of ORDEM), ESA's Meteoroid and Space Debris Terrestrial Environment Reference 2009, and the Aerospace Corporation's Aerospace Debris Environment Projection Tool. It was shown that the four models that were compared agreed to within a factor of approximately two for most debris sizes larger than 3 mm. However, the models disagreed significantly for debris smaller than 3 mm, which is also the size that poses the highest penetration risk to most spacecraft.

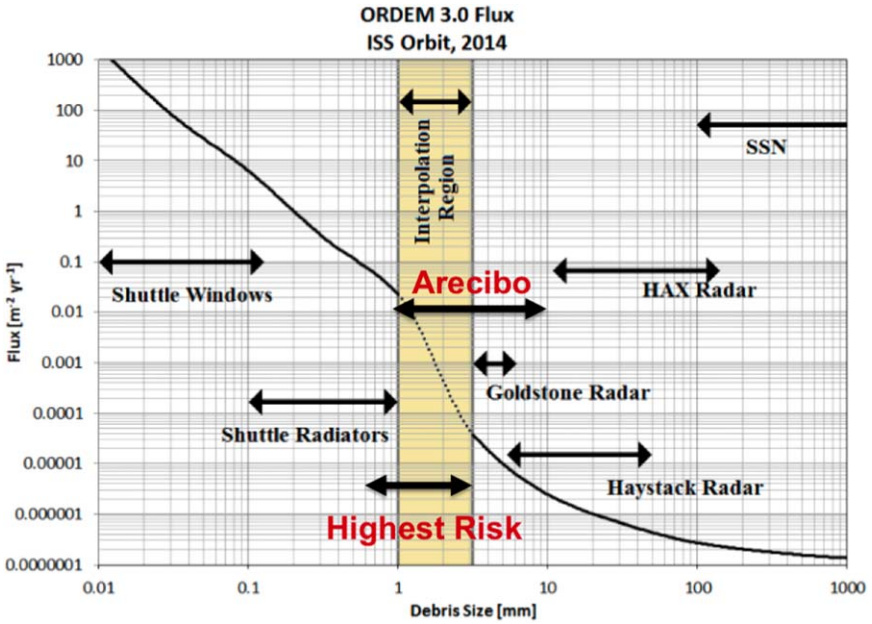

Figure 1. Cumulative flux vs. size predicted by ORDEM 3.0 with notional overlay depicting the size coverage of various ORDEM input data sets and predicted NGAT performance (Squire et al. 2015), with added overlays for emphasis. It should be noted that the figure represents the size ranges over which the measurements are estimated to be complete, not necessarily the full size range measurable by the sensors. For example, Goldstone currently measures debris between 2 and 10 mm in size, depending on altitude (Lee et al. 2020).

The Arecibo Observatory had one of the largest and most sensitive radio instruments in the world, which allowed the Arecibo Observatory to push the boundaries of knowledge in astronomy, atmospheric science, and planetary science. Unfortunately, due to the recent collapse of the Arecibo dish, now referred to as the Legacy Arecibo Telescope (LAT), much of these capabilities are no longer currently available. However, the proposal for the Next Generation Arecibo Telescope (NGAT) promises improved radar performance over the already substantive legacy system. This sensitivity could be leveraged to fill in the knowledge gaps that exist in the orbital debris environment in LEO between 1 mm and 1 cm in size, while simultaneously measuring an undersampled range of orbital inclinations. Figure 1 shows the cumulative flux versus size predicted by ORDEM 3.0 with notional overlays depicting the size coverage of various ORDEM input data sets. The figure also illustrates that the NGAT could bridge the gap between the submillimeter in-situ data and the greater than 3 mm terrestrial radar data and provide validation of orbital debris environment models in the size regime that poses the highest risk of penetration to most spacecraft.

First, we give an overview of the Arecibo Observatory and describe the systems of the LAT. We also discuss previous measurements of orbital debris and meteors using the LAT, as well as orbital debris experiments performed with other radio telescopes. Next we describe the proposed NGAT system and its improvements of interest. We describe the performance metrics of interest for orbital debris measurements and how they are calculated, using measurements performed by HUSIR for validation. We then estimate these metrics for various configurations of the LAT and NGAT and compare them to predicted HUSIR performance. Finally, we show that, with a few additional hardware upgrades to the proposed NGAT system, it would be possible to measure debris as small as 1 mm, potentially making it the most sensitive terrestrial radar for orbital debris measurements.

Table 1
General Information of the LAT (Salter 2020)

Coordinates	
Latitude	18°20′36.″6 N
Longitude	66°45′11.″1 W
Azimuth slew rate	0.°4/s
Elevation slew rate	0.°04/s
Zenith angle range	0.°0–19.°69
Reflector and Structure	
Type	Fixed reflector, movable feeds
Diameter of reflector	1000 ft (304.8 m)
Area of aperture	18 acres (73,000 m^2)
Shape of surface	70° spherical cap
Radius of curvature	870 ft (265 m)
Surface accuracy	2.2 mm rms

2. The Arecibo Observatory

The LAT was a 305 m diameter spherical dish built into a natural sinkhole near Arecibo, Puerto Rico. The dish was originally designed to be an ultra-high frequency (UHF) ionospheric radar, which featured a 430 MHz line feed suspended by steel cables at the focal line. Upgrades were made over several years, one of which included a dome containing several receivers and Gregorian optics designed to correct the spherical aberration of the original optics. Since the dish was stationary, pointing was performed by moving the receivers to different focal points above the dish. This impacted both the slew rate and the zenith angle over which the dish could point. A summary of the dish location and structure are provided in Table 1.

The Arecibo Observatory is located at 18.°3 N latitude, which is significantly closer to the equator than both the HUSIR and Goldstone Radar. As a rule of thumb, the inclination limit of a

Table 2
LAT *S*-band Radar Parameters

Operating Parameter	LAT: *S*-band
Frequency	2380 MHz
Bandwidth	10 MHz
Polarization	Circular
Peak gain	73.7 dB
Half-power beamwidth	1.9 arcmin
System temperature	20 K
Peak power	1 MW
Average power	1 MW
Max duty cycle	100%

Table 3
LAT-UHF Radar Parameters

Operating Parameter	LAT: UHF
Frequency	430 MHz
Bandwidth	2 MHz
Polarization	Circular
Peak gain	58.9 dB
Half-power beamwidth	12.24 arcmin
System temperature	66 K
Peak power	2.5 MW
Average power	150 kW
Max duty cycle	6%
Max pulse repetition frequency	1 kHz
Max pulse length	2.1 ms
Min pulse length	2 μs

radar is roughly equal to the radar latitude. We can define the fraction of visible orbital inclinations as

$$\delta i = 1 - \frac{\phi}{90^\circ}, \quad (1)$$

where ϕ is the sensor latitude. By this metric, HUSIR, Goldstone, and Arecibo can observe approximately 53%, 61%, and 80% of all possible orbital inclinations. The location of the Arecibo Observatory increases its percentage of visible orbital inclinations by 27% compared to HUSIR.

2.1. Radars of the Legacy Arecibo Telescope

2.1.1. S-band Radar

The *S*-band Radar was a planetary radar primarily used for the measurement and imaging of solar system bodies. Both the transmitter and receiver were located on the rotary floor of the dome. Diplexing was performed by rotating the transmitter out of the focus and the receiver into it. This process took a minimum of 4 s, which made it impossible to view objects in LEO. The radar could be operated in a bistatic mode to overcome this limitation.

An experiment such as this was performed in 1992 (Thompson et al. 1992) as a proof of concept for using terrestrial radar for orbital debris measurements. The receiver antenna was a 30.5 m parabolic reflector located 10.7 km north-northeast of the main antenna. The two dishes were pointed slightly off zenith such that their beam intersected at approximately 575 km and covered a range of 500–1000 km in altitude. The experiment was conducted over 3 observations for a total of 18.8 hr. During this time, 90 objects from 5 mm to 20 cm were detected for a total rate of 4.79 per hour. The size was calculated assuming metallic spheres in the Rayleigh scattering regime, as this experiment predates the NASA Size Estimation Model (SEM) for orbital debris. At the time of the experiment, the transmit power was only 400 kW. The observatory had several upgrades after this experiment, including an increase in transmission power. The most recent capabilities of the *S*-band planetary radar, prior to collapse, are shown in Table 2.

2.1.2. UHF Radar

The UHF radar was primarily an incoherent scatter radar used to study the ionosphere. The radar has also been used for measurements of the moon, near-Earth asteroids, and meteors. The first reported use of the system for meteor observations was reported in 1995 (Zhou et al. 1995) where meteor ablation trails were observed in the 80–120 km altitude range. Since then, additional observations have been performed and analysis techniques have been developed by Zhou & Kelley (1997), Janches et al. (2000), Sulzer (2004), Wen et al. (2004), Wen et al. (2005a), Wen et al. (2005b), and Briczinski et al. (2009) proving the UHF radar of the LAT to have been a crucial instrument to the study of radar meteors.

Power from the UHF transmitter could be routed to the line feed, the dome feed, or both simultaneously in a dual beam or *dual radar* configuration by way of a power splitter. The line feed had greater gain at zenith than the dome feed due to its greater aperture filling factor. As the line feed moved away from zenith, the gain decreased and the system temperature increased due to illumination spillover. Although this happened to some extent with the dome feed, the effect was diminished because the dome feed illuminated a smaller portion of the dish. The most recent capabilities of the UHF radar, prior to collapse, are shown in Table 3.

2.2. Receivers of the Legacy Arecibo Telescope

The Arecibo Observatory had receivers that spanned in frequency from high frequency to *X*-band, the parameters of which are shown in Table 4. These receivers could be used as the receiver antennas for a bistatic radar configuration. An experiment using a radio telescope as a receiver in a bistatic system for the detection of orbital debris was performed in 1997 (Leushacke et al. 1997) using the Tracking and Imaging Radar (TIRA) operated by the Research Establishment for Applied Science, commonly referred to as FGAN, and the Effelsburg Radio Telescope operated by the Max Planck Institute for Radio Astronomy.

TIRA is a 34 m *L*-band monopulse radar that is located 21 km from the 100 m diameter Effelsburg Radio Telescope. In the experiment, named COBEAM-1/96, the dishes were pointed to intersect at an altitude of 850 km with an altitude window that ranged from 750 to 980 km. During the 24 hour observation, 317 objects were detected yielding a detection rate of 13.02 per hour. The minimum-detectable size at Effelsburg was approximately 1 cm using 32 integrated pulses. This is a factor of two improvement over the TIRA monostatic limit of 2 cm at 1000 km using 64 integrated pulses. One of the main drawbacks of COBEAM-1/96 was Effelsburg's lack of a monopulse receiver. This meant that the authors could not correct for the off-boresight attenuation and could only report a minimum possible size of the debris.

Table 4
Receivers of the LAT (NAIC 2020)

Name	Frequency Range (GHz)	Native Polarization	Gain (K Jy^{-1})	Temp. (K)	Beam Size (arcmin)
CH 47—MHz	***	Dual circular	***	***	110 × 94
327—MHz	0.312–0.342	Dual linear	11	113	15 × 14
CH 430—MHz	0.425–0.435	Dual circular	20	120	9.5 × 8.5
430—MHz	0.422–0.442	Dual circular	11	50	12 × 10
ALFA	1.225–1.525	Dual linear	10	30	3.8 × 3.3
L-wide	1.15–1.73	Dual linear	10	33	3.5 × 3.1
S-low	1.8–3.1	Dual linear	8	40	2.0 × 1.8
S-narrow	2.33–2.43	Dual circular	10	25	2.0 × 1.8
S-high	3.0–4.0	Dual linear	8.5	34	1.5 × 1.35
C	3.85–6.00	Dual linear	6	34.5	1.0 × 0.9
X	7.8–10.2	Dual circular	4	30	0.57 × 0.5

Improved debris observation campaigns were performed in 2006 and 2007 (Ruiz et al. 2006) using TIRA and a multibeam receiver at the Effelsburg Radio Telescope, a receiver similar to that of the ALFA multibeam receiver of the LAT. The experiments, MBPE-1/06 and MBPE-1/07, had minimum-detectable sizes similar to that of COBEAM-1/96. Using the algorithms for the path estimation through multibeam receivers (Ruiz et al. 2005), they were able to produce path estimates for objects as small as 3.55 cm at 1390 km (Letsch et al. 2009).

Numerous other radio telescopes have also been proposed for the study of orbital debris. A proposal to use the Sardinia Radio Telescope in this regard was made in 2005 (Saba et al. 2005). A sensor pair dubbed the Bistatic Radar for LEO Tracking used the Sardinia Radio Telescope and the Flight Termination System (FTS) of the Italian Joint Test Range of Salto di Quirra to perform observations of cataloged objects in 2017 (Muntoni et al. 2017). Another system, Bistatic Radar for LEO Survey, proposed using the FTS and the multibeam Northern Cross Radio Telescope and performed simulated observations of cataloged objects in 2015 (Morselli et al. 2014). Several papers describing experiments using the Evpatoria RT-70 transmitter and the Medicina Radio Telescope have also been published. One paper in 2001 (Zaitsev et al. 2001) proposed the measurement of centimeter-sized objects in the Geostationary Ring. Observations performed in 2008 (Pupillo et al. 2008) indicate that the Medicina-Evpatoria pair has the the potential to observe centimetric to subcentimetric debris in LEO.

3. Next Generation Arecibo Telescope

On 2020 December 1, the LAT unexpectedly collapsed. In its 57 yr, the LAT's unique capabilities contributed significantly to three separate major scientific areas: planetary science, space and atmospheric sciences, and astronomy. In the wake of the collapse, a team of scientists and engineers have begun to envision the future of the Arecibo Observatory. A white paper was released describing the concept for the NGAT, which features a larger frequency coverage, higher gain, more transmit power, and a greater field of view, among other improvements (Roshi et al. 2021).

To meet the science requirements of large sky coverage, large collection area, excellent surface brightness sensitivity, and several megawatts of transmitting power, a *compact dish array on a single plane* design was chosen. Two variations of the design are an array of 1112 dishes of 9 m in diameter within a 314 m diameter circle and an array of 400 dishes of 15 m diameter within a 331 m diameter circle. It is also proposed that the signals from each dish be digitized as near to the receiver as possible, with the suggestion that spatial-radio-frequency nulling and grating lobe suppression could be performed with proper element weighting. The estimated gain and transmit power of the NGAT at UHF, *S*-band, and *C*-band are shown in Table 5.

Table 5
Estimated Gain and Transmit Power of the NGAT

	UHF	*S*-band	*C*-band
Frequency	430 MHz	2380 MHz	5000 MHz
Gain	61.5 dB (20 K Jy^{-1})	76.4 dB (20 K Jy^{-1})	82.4 dB (18 K Jy^{-1})
Transmit power	10 MW	5 MW	5 MW

4. Performance Metrics

There are various bistatic and monostatic configurations in which the LAT and NGAT could and can be used for orbital debris measurement. Three key performance metrics for evaluating the utility of any particular configuration are the minimum-detectable debris size, the total debris detection rate, and the number of pulses expected on an object when it crosses the beam. Here we provide a brief description of these parameters and their method calculation. A detailed mathematical derivation is deferred to Appendix.

Radar does not directly measure the size of an object, but rather measures an object's radar cross section (RCS). A target's RCS depends not only on the size but also on the reflectivity of its surface and the directivity of the radar reflection caused by the target's shape. To relate RCS to size, we use the NASA-SEM. This model creates a one-to-one mapping of RCS to size for radar measurements of orbital debris (Xu et al. 2005). Knowing the transmitter and receiver properties of a radar, one can use the bistatic radar equation along with a choice of signal-to-noise ratio (S/N) threshold to estimate a minimum-detectable RCS. This is then related to a minimum-detectable size via the NASA-SEM. Since minimum-detectable RCS and size are altitude dependent, we choose to present these parameters at a standard altitude of 1000 km.

Estimates of the total debris detection rate are important considerations even with an excellent minimum-detectable size; one must be able to obtain statistically significant data in a reasonable amount of time. While the minimum-detectable size mostly depends on the radar sensitivity, the total debris

Table 6
Summary of HUSIR Data Taken in 2018

	HUSIR
Observation Time in 2018	313.2 hr
Total number of detections in 2018	4964 detections
Measured detection rate in 2018	15.85 per hour

detection rate also depends on the geometry of the beam intersection and the actual flux of debris on orbit. To estimate debris flux, we use NASA's ORDEM (Stansbery et al. 2014). ORDEM can be used in "Telescope Mode" to estimate debris flux as a function of size and altitude using a radar's location and pointing direction. We then translate this to a *detectable* debris flux through the calculation of a probability of detection as a function of size and altitude, interpreted as the fraction of debris detected of each size at each altitude. This detectable debris flux is then multiplied by the altitude-dependent beam-intersection area of the radar to calculate a total count rate of detectable debris. Here the total debris detection rate is integrated from 400 to 2000 km altitude for each instrument.

While large apertures and higher frequencies increase the sensitivity for debris observations, they also narrow the beam of the radar. Since debris observations are performed in a beam-park mode, the number of pulses expected on an object as it crosses the beam is dependent on the width of the beam, the speed of the object through the beam, and the pulse repetition frequency (PRF) of the radar. For a maximum unambiguous range of 2000 km, the necessary PRF for a continuous-wave (CW) pulse is approximately 75 Hz. Since the speed of the object is altitude dependent, the number of pulses expected is estimated at the beam-intersection altitude of 1000 km assuming the object crosses through the center of the beam and the radar uses a PRF of 75 Hz.

5. Detection Rate and Minimum-detectable Size Estimates for the LAT and NGAT

5.1. HUSIR Predictions and Validation

Results published by NASA (Murray & Kennedy 2020) for data taken in 2018 are used as a validation source. Total observation time, number of detections, and corresponding detection rate are shown in Table 6. Predictions based on the previously described methods are shown in Table 7. Our estimates are within approximately 2% of the reported detection rate for that year, indicating the detection rate calculation is performing well. Additionally, our calculated minimum-detectable size of 5.43 mm matches well with the reported 5.5 mm minimum size. The average number of pulses expected on an object at 1000 km is 8.59.

5.2. Monostatic

The UHF radar was the only LAT configuration that could act monostatically for debris detection. The ideal operating characteristics of the transmitter are detailed in Table 3. Table 8 shows that in this configuration the LAT could detect objects as small as 1.4 cm at 1000 km altitude, while the NGAT could detect objects as small as 9.3 mm. In both cases, more than 4 times the number of pulses are expected than HUSIR. While not as sensitive as HUSIR, these configurations would still be among the most sensitive instruments used for these kinds of

Table 7
Predicted HUSIR Performance for 2018 Observations

	HUSIR
Minimum RCS @ 1000 km	−47.34 dBsm
Minimum size @ 1000 km	5.43 mm
Intersection area	6 303.95 km^2
Total count rate	16.07 per hour
Number of Pulses @ 1000 km (75 Hz)	8.59

Table 8
UHF-monostatic Performance

	LAT: UHF	NGAT: UHF
Minimum RCS @ 1000 km	−75.94 dBsm	−87.26 dBsm
Minimum size @ 1000 km	14.4 mm	9.30 mm
Intersection area	14 166.65 km^2	14 166.65 km^2
Total count rate	3.66 per hour	7.76 per hour
Number of Pulses @ 1000 km (75 Hz)	36.32	36.32

Table 9
VLBI Receiver Parameters (Perilat 2020)

Operating Parameter	VLBI
Frequency	2380 MHz
Gain	47.2 dB (0.024 K Jy^{-1})
T_{sys}	107 K
HPBW	0.°665
Coordinates	18°20′53.″9 N, 66°45′5.″7 W

measurements. Additionally, there exists the opportunity to perform commensal observations with the existing ionospheric measurements. In Zhou et al. (1995), the echoes from meteor ablation trails between 80 and 120 km altitude that were considered "noise" in the ionospheric measurements turned out to be a fortuitous source of meteor observations. Methods were developed in Wen et al. (2005a) to filter meteors from the ionospheric data, to "clean" the data, and to produce a commensal meteor-detection data set. Similar techniques can be developed for the detection of orbital debris at higher altitudes providing useful data with little additional overhead.

Several data sets taken with the LAT already exist and are available from the Arecibo Observatory Data Archive. Even without new observations from the NGAT, there exists the opportunity to extract useful orbital debris data from the instruments of the Arecibo Observatory.

5.3. VLBI Reference Antenna

The Arecibo Observatory has a 12 meter antenna located approximately 450 m north of the center of the main dish. The antenna was built to act as a reference antenna for calibration when the LAT's main dish was used for very long baseline interferometry (VLBI). The characteristics of the VLBI reference antenna are summarized in Table 9. Since the 12 meter antenna is so close to the main dish and the receiver beamwidth is comparatively large, the beams nearly entirely overlap. This could be described as a quasi-monostatic configuration. Assuming a 3 ms CW pulse, in this configuration, the LAT could detect an 8 mm object at 1000 km altitude, as shown in Table 10. Although the minimum-detectable RCS is higher than that of the UHF-monostatic configuration, the minimum-detectable size is smaller because of the increased

Table 10
VLBI Performance

	LAT: *S*-band	NGAT: *S*-band	NGAT: *C*-band
Minimum RCS @ 1000 km	−61.45 dBsm	−71.14 dBsm	−77.69 dBsm
Minimum size @ 1000 km	8.00 mm	5.51 mm	2.61 mm
Intersection area	3 509.88 km^2	3 509.88 km^2	1 668.72 km^2
Total count rate	2.23 per hour	6.14 per hour	63.14 per hour
Number of Pulses @ 1000 km (75 Hz)	7.83	7.83	3.74

RCS to size *efficiency* of the *S*-band as compared to the UHF in the Rayleigh scattering regime.

Using the NGAT at *S*-band would allow the detection of debris as small as 5.5 mm at 1000 km altitude, roughly the same sensitivity as HUSIR. The number of pulses expected at 1000 km, 7.83, is also comparable to HUSIR. The VLBI reference antenna does not currently have a *C*-band receiver. However, if one with similar noise and gain parameters were to be installed, a minimum-detectable size of 2.6 mm at 1000 km with a total count rate of 63 hits per hour would be achievable. While the number of expected pulses decreases to 3.74, this is still greater than the three- and two-pulse minimums employed by HUSIR and Goldstone, respectively, for detection validation. This level of performance is comparable to the Goldstone Orbital Debris Radar, the most sensitive radar used for orbital debris measurements in LEO.

The Goldstone Orbital Debris Radar is a bistatic radar that used Deep Space Station 14 (DSS-14) as a transmitter and DSS-15 as a receiver until it was decommissioned in 2018 (Murray 2019). While new Goldstone configurations with a comparable sensitivity have been employed, the instantaneous altitude coverage for a given intersection altitude was reduced from a 280 to 3000 km window to a 300 km window within 600–1000 km (Lee et al. 2020) due to the increased bistatic baseline. Since this configuration of the NGAT is able to view all LEO altitudes simultaneously, it could recreate the performance of the legacy Goldstone system.

5.4. VLBA Antenna St. Croix

On St. Croix in the Virgin Islands, there is an antenna that is part of the Very Long Baseline Array (VLBA). It is located 238 km southwest of the Arecibo Observatory. The dish has a larger aperture and lower system temperature than the 12 meter antenna on site, as seen in Table 11. Table 12 shows that in this configuration at *S*-band the LAT could detect a 5.5 mm object at 1000 km altitude, while the NGAT could detect a 3.8 mm object. The altitude coverage from beam-null to beam-null at 1000 km is approximately 56 km. Even with the small intersection area, This configuration would manage a detection rate of 0.4 per hour. The expected number of pulses at 75 Hz PRF is similar to the VLBI configuration. However, the PRF, and consequently the number of pulses, could be nearly doubled since the maximum unambiguous range need only extend as far as the highest altitude of the beam overlap, approximately 1028 km.

At *C*-band, it would be possible to detect objects with sizes down to 1.7 mm. Even though the intersection area is small, debris flux increases rapidly below 3 mm resulting in a reasonable detection rate of 4.4 per hour. Although multiple pointings would be required for a full survey of LEO, the sensitivity afforded by this bistatic arrangement would provide unprecedented terrestrial radar data of the debris environment.

Table 11
VLBA Receiver Parameters (Romney 2019)

Operating Parameter	VLBA
Frequency	2380 MHz/5000 MHz
Gain	52.7 dB/60.6 dB (0.087 K/Jy/0.119 K/Jy)
T_{sys}	40 K
HPBW	0.°352/0.°074
Coordinates	17° 45′23.5 N, 64° 35′1.″5 W

5.5. Green Bank Radio Telescope

The Green Bank Radio Telescope (GBT) is located in Green Bank, West Virginia. It is the largest fully steerable radio telescope in the world and has the lowest system temperature of all the receivers mentioned in this paper. The receiver parameters of the GBT at *S*-band and *C*-band are given in Table 13.

As shown in Table 14, in this configuration, the LAT could detect a 4.0 mm object at 1000 km, making it more sensitive than HUSIR. At *S*-band the NGAT could detect objects as small as 2.8 mm. At *C*-band the NGAT would be able to detect objects down to 1.3 mm, the smallest size yet. Although great for sensitivity, the large aperture and correspondingly narrow beam of the GBT as well as the large geographic separation drastically reduce the intersection area. The altitude coverage of this configuration from beam-null to beam-null at 1000 km is approximately 10 km. At *C*-band the altitude coverage is too small (more narrow than the altitude bins of ORDEM output) to allow for an accurate estimation of the total count rate. Due to the diminished instantaneous altitude coverage, this configuration would be more useful to perform targeted follow-up observations of an on-orbit breakup. Additionally, due to the elevation limits of the GBT, only altitudes above 800 km could be observed.

6. NGAT Design Suggestions

While the presented NGAT design has appreciable potential for performing measurements of orbital debris, there are four design suggestions that would significantly improve the performance of the NGAT for statistical sampling of the debris environment in LEO. These are as follows: fast transmit-receive switching enabling monostatic LEO observations, multibeam-receiver capabilities for a path through the beam estimation, digital pulse modulation to increase PRF through inter-pulse binary coding, and a high-dynamic-range receiver for the measurement of debris over orders of magnitude in size.

Fast transmit-receive switching would allow for monostatic observations of LEO at *S*- and *C*-band frequencies. This would maximize sensitivity by using the superb gain of the NGAT on reception as well as transmission. In order to measure debris at 400 km altitude, the nominal orbit altitude of the International

Table 12
VLBA Performance

	LAT: *S*-band	NGAT: *S*-band	NGAT: *C*-band
Minimum RCS @ 1000 km	−70.87 dBsm	−80.57 dBsm	−88.54 dBsm
Minimum size @ 1000 km	5.57 mm	3.84 mm	1.72 mm
Intersection area	47.25 km^2	47.25 km^2	10.70 km^2
Total count rate	0.10 per hour	0.40 per hour	4.44 per hour
Number of Pulses @ 1000 km (75 Hz)	7.83	7.83	3.74

Table 13
GBT Receiver Parameters (GBT Scientific Staff 2021)

Operating Parameter	GBT
Frequency	2380 MHz/5000 MHz
Gain	66.4 dB/72.9 dB (2.0 K/Jy)
T_{sys}	18 K/18 K
HPBW	5′.8/1′.2
Coordinates	38°25′59″.2 N, 79°50′23″.4 W

Space Station, the NGAT would need to start receiving echoes at approximately 2.7 ms from the leading edge of the pulse. If the HUSIR debris waveform is copied with a pulse length of 1.6384 ms, the necessary switching time is approximately 1 ms. This is not possible by physically rotating the transmitter and receiver in and out of the focus as was done with the LAT Planetary Radar. Some form of electronic switching or circulator circuit would be necessary, which would unfortunately reduce isolation and raise the system temperature. However, even assuming a pulse length and system temperature similar to HUSIR, the NGAT would still be capable of detecting millimeter-sized objects at 1000 km altitude, as shown in Section 7.

In statistical LEO debris observations, like the ones discussed thus far, the radar points in a single direction and measures objects as they pass through the radar beam. Since the objects fly randomly through the beam, not necessarily through the antenna boresight, knowledge of the path taken by the object through the beam can be used to correct for off-axis beam shape losses to obtain a more accurate integrated RCS measurement. Knowledge of the path through the beam can also be used to estimate the orbital inclination of the debris. HUSIR performs this path through the beam estimation using information from the difference channels of a monopulse receiver. A monopulse receiver provides an angular offset measurement for each pulse using the differences between four or more squinted beams from the receiver horn. Methods for paths through the beam estimation with multibeam receivers in a bistatic radar system have been discussed in Morselli et al. (2014), Ruiz et al. (2006), Letsch et al. (2009), and Ruiz et al. (2005). To use similar techniques, the NGAT would need to provide a minimum of four receive beams to perform a similar path through the beam estimates.

One way to increase the number of expected pulses on an object is to increase the PRF of the radar. The PRF is typically limited by the desired maximum unambiguous range. However, one can increase the PRF without reducing the unambiguous range through a technique known as inter-pulse binary coding (Levanon 2009). By interleaving a series of uniquely modulated pulses, one can associate each radar return to its original pulse repetition interval, decoupling the range ambiguity from the PRF. Increasing the number of pulses on an object increases the total energy on the target within the beam-crossing time interval improving the sensitivity as well as the number of pulses that could be used to estimate the path through the beam. In the bistatic case, this can be taken to the extreme by transmitting continuously, since the transmitter does not have to cease transmitting in order to listen for echoes as it does in the monostatic case. Other forms of pulse compression, such as chirped signals, could also be employed to increase the metric accuracy of individual measurements, since pulsed-CW waveforms typically have lower-range resolution. The incorporation of digital pulse modulation would allow the implementation of these techniques, improving the performance of the radar for statistical debris observations.

One final important aspect is the dynamic range of the receiver. While the majority of debris objects coming through the radar beam would be small, occasionally large objects may pass through the beam, causing the receiver to saturate and result in an underestimate of the debris object's true size. In particular, orbital debris data from the Goldstone Orbital Debris Radar has shown that the limited dynamic range affects the measurement of large debris, effectively limiting Goldstone's practical, measured size distributions to smaller than 1 cm (Murray et al. 2019b). HUSIR increases its dynamic range through the use of an automatic gain control (AGC) unit. When a signal begins to saturate the receiver, attenuation is applied to the receive signal automatically to prevent further saturation of the front-end receivers. This allows HUSIR to measure objects as small as approximately 5 mm at 1000 km to as large as several meters. While some form of AGC would be ideal, it is only necessary that the receiver have enough dynamic range to measure large enough objects to overlap with existing data sources.

For radar, we define dynamic range as the ratio of maximum signal power for which the receiver is not saturated to the minimum signal power for which the receiver still detects something. This corresponds to the largest object at the lowest altitude and the smallest object at the highest altitude, or

$$D = \frac{P_{\max}}{P_{\min}} = \frac{\sigma_{\max} R_{\max}^4}{\sigma_{\min} R_{\min}^4}. \quad (2)$$

We can invert the NASA-SEM to determine the corresponding RCS at a size of interest. For excellent overlap, we would want to measure from roughly 1 mm to 10 cm in size. Coverage from 1 mm to 1 cm would give a similar large-size overlap as the Goldstone Orbital Debris Radar. Coverage from 1 to 5.5 mm would be about the minimum size range necessary to overlap with HUSIR data. Assuming we want to measure from 400 to 1000 km with no distortion, each of these size ranges (1 mm to 10 cm, 1 mm to 1 cm, and 1 to 5.5 mm) would require 111, 76, and 60 dB of dynamic range, respectively.

Table 14
GBT Performance

	LAT: *S*-band	NGAT: *S*-band	NGAT: *C*-band
Minimum RCS @ 1000 km	−79.5 dBsm	−89.19 dBsm	−95.79 dBsm
Minimum size @ 1000 km	4.00 mm	2.76 mm	1.31 mm
Intersection area	6.87 km^2	6.87 km^2	2.05 km^2
Total count rate	0.04 per hour	0.18 per hour	***
Number of Pulses @ 1000 km (75 Hz)	7.60	7.60	3.62

7. Detection Rate and Minimum-detectable Size Estimates for a Monostatic NGAT

While the anticipated increases to both gain and transmission power do improve performance for the bistatic configurations outlined in the preceding sections, the estimation of monostatic performance is still of interest. The current design of the NGAT still does not allow for monostatic operation of the planetary radar for LEO observations. It is mentioned in the NGAT white paper that the addition of fast transmit-receive switching to the planetary radar would allow for the measurement of millimeter-sized orbital debris in LEO. Here we verify and quantify these claims by calculating minimum-detectable sizes and debris detection rates, assuming monostatic operation with a 1.638 4 ms transmit pulse, such as that used by HUSIR.

If the NGAT could incorporate fast switching, its superior gain could be leveraged on reception as well as transmission, significantly increasing its sensitivity for LEO debris measurements. Since this kind of switch would likely increase the system temperature of the receiver, we assume a similar system temperature as that of HUSIR for our calculations: 186 K. With this assumption, the NGAT could detect objects as small as 2.2 mm at *S*-band, as shown in Table 15. This is even smaller at *C*-band, approximately 1 mm, which completely bridges the gap between on-orbit and terrestrial LEO debris measurements. Because the modeled flux increases significantly between 1 cm and 1 mm, the predicted count rate is approximately 6.6 detections per minute at *S*-band and 1.1 detections per second at *C*-band. Additionally, although the monostatic beam is more narrow, a sufficient number of pulses can still be collected on an object as it crosses the beam.

Table 15
NGAT Monostatic Performance: *S*-band and *C*-band

	NGAT: *S*-band	NGAT: *C*-band
Minimum RCS @ 1000 km	−95.15 dBsm	−100.77 dBsm
Minimum size @ 1000 km	2.19 mm	1.08 mm
Intersection area	2 559.43 km^2	1 218.29 km^2
Total count rate	394.03 per hour	3 973.17 per hour
Number of Pulses @ 1000 km (75 Hz)	5.64	2.97

8. Conclusions

There exist gaps in the empirical knowledge of the debris environment: millimetric debris in LEO, low-inclination debris in LEO, and centimetric debris in GEO. In this paper, we have described and developed methods for estimating key debris observation parameters: minimum-detectable RCS, minimum-detectable size, observational surface area for bistatic radar, number of expected pulses on an object, and total debris detection rates. These observation parameters were estimated for debris observations taken by the HUSIR radar in 2018 and shown to be in agreement.

It has been demonstrated that the LAT and NGAT could be used to fill many gaps of empirical knowledge of the debris environment. The location of the Arecibo Observatory would provide access to 27% more orbital inclinations than HUSIR. There exists data from the LAT in the Arecibo Observatory Data Archive from which useful measurements of centimeter-sized debris at low inclinations can be extracted. The NGAT could also gather significant amounts of data on centimeter-sized debris through commensal observations. One NGAT bistatic arrangement could have a sensitivity comparable to the Goldstone Orbital Debris Radar while observing at all LEO altitudes in a single pointing. Another bistatic arrangement could provide measurements of debris as small as 1.7 mm.

Four design suggestions that would significantly improve the performance of the NGAT for statistical sampling of the debris environment in LEO were presented: fast transmit-receive switching enabling monostatic LEO observations, multibeam-receiver capabilities for paths through the beam estimation, digital pulse modulation to increase PRF through inter-pulse binary coding, and a high-dynamic range receiver for the measurement of debris over orders of magnitude in size. With the proposed design suggestions, the NGAT could detect objects as small as 1 mm at 1000 km. This would completely bridge the gap between on-orbit in-situ debris measurements and terrestrial radar debris measurements.

Ultimately, we have shown that data from the LAT and NGAT can be used significantly to improve the short-term debris environment models that are used to inform spacecraft design and operations, ultimately reducing the potential risk to space operations.

Appendix
Performance Metric Calculation Details

A.1. Minimum-detectable Radar Cross Section

The radar equation generalized for bistatic radar is given by Skolnik (1990) as follows:

$$P_r = P_t \frac{G_t G_r \sigma \lambda^2}{(4\pi)^3 R_t^2 R_r^2}, \tag{A1}$$

where P is power, G is gain, R is the slant range, λ is the wavelength, and σ is the bistatic RCS. The t and r subscripts refer to the transmitter and receiver respectively. Assuming that the primary noise contribution comes from thermal noise in the receiver, we can divide the expression by the receiver noise power to obtain an expression for the S/N. Including system losses, the expression can then be rearranged to isolate the

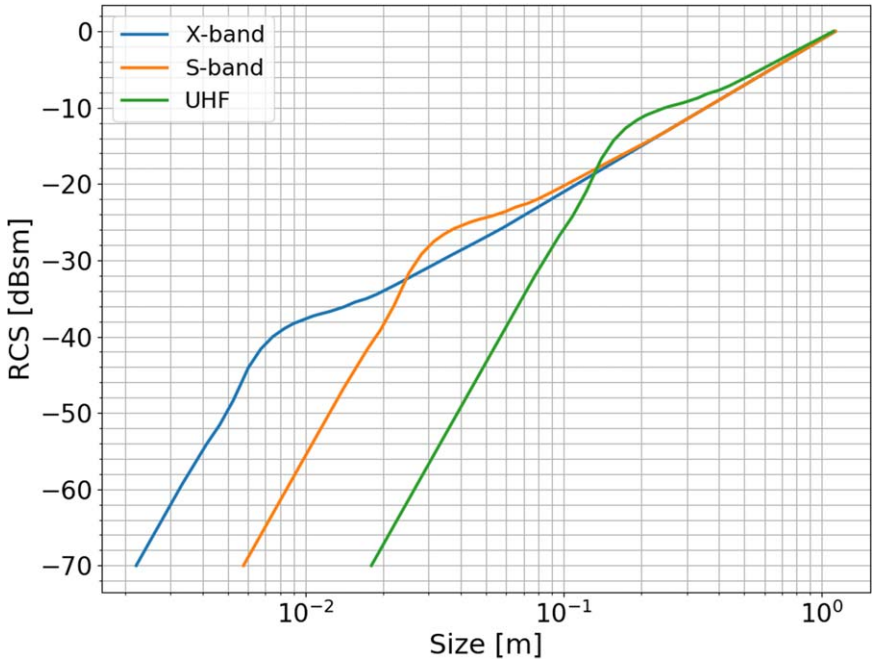

Figure 2. NASA-SEM for UHF, *S*-band, and *X*-band: RCS to size conversion.

minimum-detectable RCS, which gives

$$\sigma_{\min} = \mathrm{S/N}_{\min} \frac{(4\pi)^3 R_t^2 R_r^2 k_B T_{sys} \Delta f_r L}{P_t G_t G_r \lambda^2}, \tag{A2}$$

where T_{sys} is the receiver system temperature, k_B is Boltzmann's constant, Δf_r is the receiver bandwidth, and L is the total system loss. The total system loss is a combination of losses including transmit losses, receiver losses, atmospheric losses, scanning losses, range-gate straddling losses, Doppler straddling losses, collapsing losses, signal processing losses, and other miscellaneous losses. Here we have chosen to include an average loss of 9 dB to account for all of these factors. Additionally, we define $\mathrm{S/N}\min = 10$ dB. It should be noted that this applies to a single-pulse detection at the peak gain of both the transmitter and receiver.

A.2. Minimum-detectable Size

The size estimation is based on the ODPO-SEM. This model creates a one-to-one mapping of RCS to the characteristic length/size, where the characteristic length is defined as the average of the three longest orthogonal lengths of an object. Details of the SEM are given in Xu et al. (2005). An example of the NASA-SEM for UHF, *S*-band, and *X*-band is shown in Figure 2.

A.3. Observational Surface Area

In a bistatic radar, the observation volume is confined to the intersection of the transmitter beam and the receiver beam. Calculating the intersection volume is a common problem in experiments where multiple transmitters and receivers are illuminating/observing the same volume. An analytic solution for intersecting cylinders has been given by Hubbell (1965). Analytic solutions to symmetric congruent cones have been given in Hughes & Clamons (1974) and Beyer et al. (1987). Several numeric approaches were presented in Balogun et al. (2000) for the general intersection of two cones.

Although a similar problem, the calculation needed here is not the volume of the intersection, but surface area of the surface defined by the intersection of the two volumes. Additionally, the calculations need not just the total surface area, but surface area as a function of altitude because orbital debris flux is not uniform in altitude. The approach taken involves calculating the product of the normalized gain of each antenna at discrete points in full 3D on a WGS-84 Earth ellipsoid.

To calculate the lateral surface area between two slant ranges (as determined by the start and stop altitudes desired), one begins by choosing a set of N points $\{(x_i, y_i)|i = 0, 1,\ldots,N-1\}$ on a grid in a plane perpendicular to the boresight vector of one antenna. Then for each point, the angular offset from each antenna θ is calculated as

$$\theta_{i,j} = \arccos \frac{\boldsymbol{r}_{i,j} \cdot \boldsymbol{b}_j}{|\boldsymbol{r}_{i,j}||\boldsymbol{b}_j|}, \tag{A3}$$

where $\boldsymbol{r}_{i,j}$ is the vector from the jth antenna to the ith point in the plane and $\boldsymbol{b}_j$ is the boresight vector of the jth antenna. Then the convex hull of points within the beam is taken where *in the beam* is defined as where the normalized gain product of the two antennas is greater than −6 dB, which can be represented as

$$H = \mathrm{ConvexHull}((x_i, y_i)| \prod_{j=1,2} G_j(\theta_{i,j}) \geqslant 0.25) \tag{A4}$$

where $G_j(\theta)$ is the normalized gain pattern of the jth antenna as a function of the angular offset from boresight. Here we model each antenna as a uniformly illuminated circular aperture where the pattern produced is well known as an Airy disk and is given by

$$G(\theta) = \left(\frac{2J_1(ka \sin\theta)}{ka \sin\theta} \right)^2, \tag{A5}$$

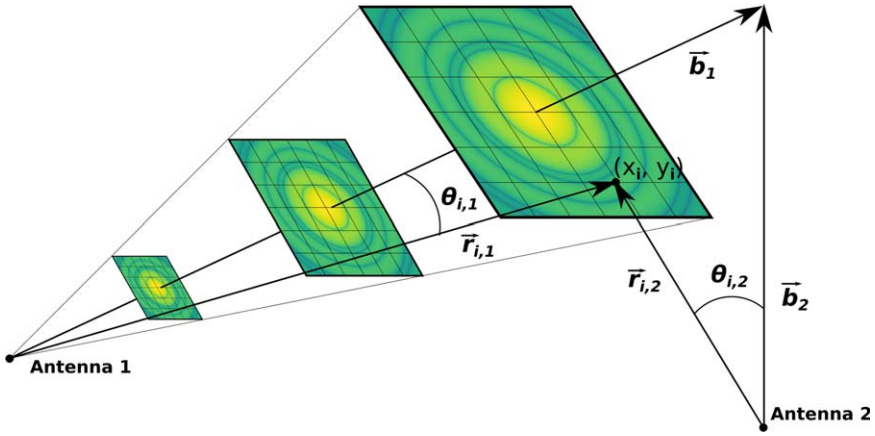

Figure 3. Geometry used for the calculation of the lateral surface area of the beam intersection.

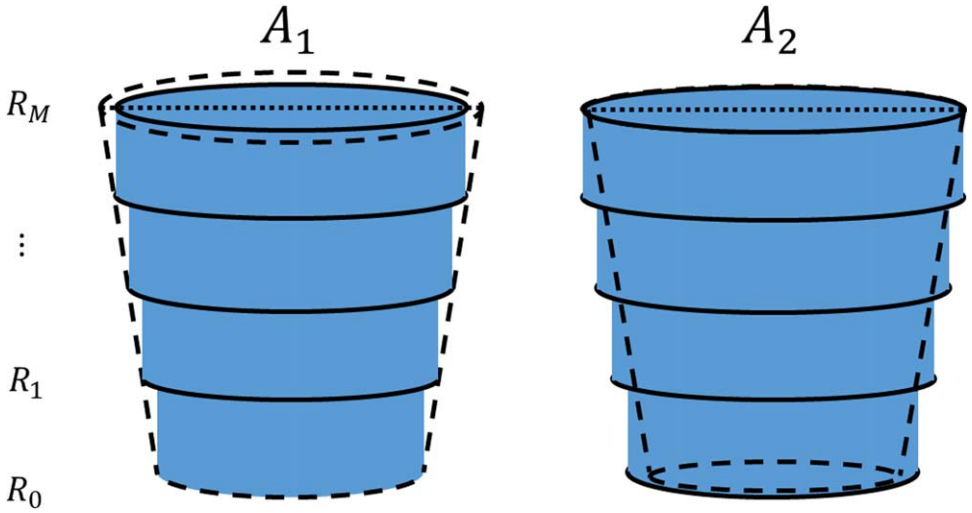

Figure 4. Examples of overestimates and underestimates of lateral surface area. Here a conic frustum is used as the example 6 dB surface for simplicity.

where J_1 is the Bessel function of the first kind of order one, $k = 2\pi/\lambda$ is the wavenumber, a is the radius of the aperture, and θ is the angular offset from the normal vector of the aperture. Although an Airy disk has been chosen here, any axis-symmetric beam pattern can be used. An illustration of the geometry discussed can be found in Figure 3.

The convex hull of a set of points is the smallest convex set that contains the points. There are many algorithms for calculating a convex hull. Here we use the Qhull algorithm (Barber et al. 1996), specifically the SciPy (Virtanen et al. 2020) implementation. In addition to returning the points comprising the convex hull, QHull returns the surface area and volume of the hull, or perimeter and area if the hull is 2D.

Once the perimeter of the 6 dB surface in the plane is calculated, we approximate the lateral surface area of the beam overlap between this plane and the next as a polygonal cylinder whose lateral surface area is the product of the perimeter of its base and its height, i.e., the distance between the two planes. As shown in Figure 4, when calculating the lateral surface area between two planes, one can choose the base of the approximating cylinder to be in either the bottom or top plane, resulting in an underestimate or overestimate of the true area of the surface depending on the relative values of the perimeter in each plane.

To improve accuracy, we effectively take an average of the two. For an approximation using M cylinders, assuming equally spaced planes, the area is calculated as

$$A = \sum_{i=0}^{M-1} (P(R_i) + P(R_{i+1})) * \frac{(R_M - R_0)}{2M} \quad \text{(A6)}$$

where $P(R_i)$ is the perimeter of the 6 dB surface in the plane at a range R_i, R_0 is the range corresponding to the start altitude, R_M is the range corresponding to the stop altitude, and M is the number of cylinders. The final area is calculated by multiplying by the cosine of the local angle with respect to the vertical.

ORDEM flux output for LEO, further discussed in Section A.4, can be binned in either 50 km or 5 km wide bins. Here we use the 5 km bin size to better capture the bistatic effects on sensitivity and area as a function of altitude. For the area calculations here, we use 25 approximating cylinders per altitude bin with 62,500 (250^2) points sampled in each plane.

A.4. Debris Detection Rate

NASA publishes a software called ORDEM, currently in its third version (Stansbery et al. 2014), with the most recent release being ORDEM 3.1. ORDEM can be used in "Telescope

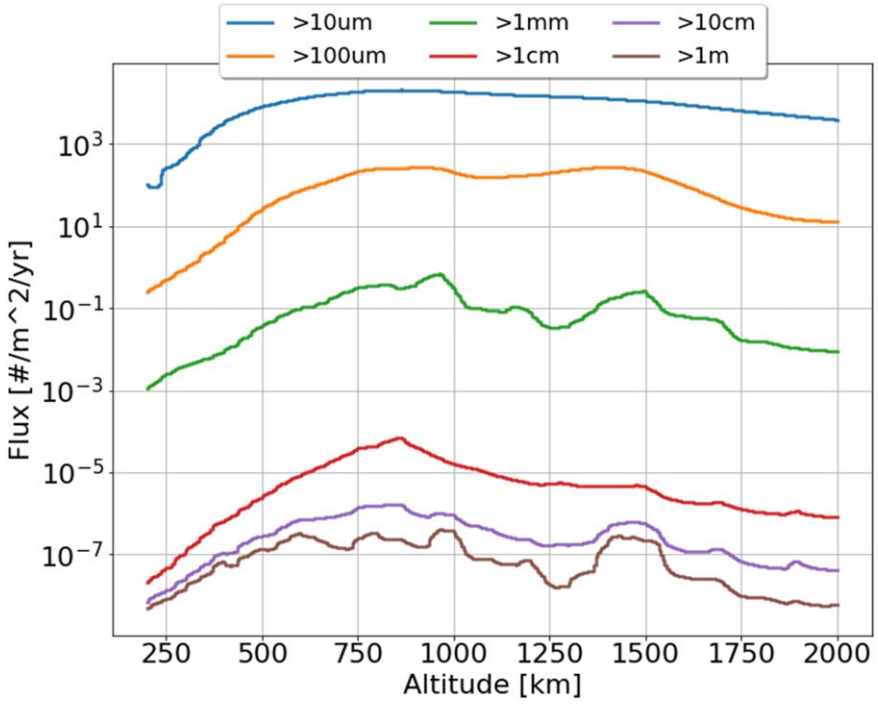

Figure 5. Cumulative flux of debris to decadal limiting sizes as computed by ORDEM for a sensor located at 18°.444 latitude pointed at 90° elevation in 2018.

Mode" to retrieve the modeled debris flux as a function of altitude and debris size for a radar using the radar's geographic coordinates and its pointing direction. A representative ORDEM output is shown in Figure 5. The flux calculated by ORDEM is the flux through the lateral surface area of a conical frustum whose opening angle is the 2-way 6 dB beamwidth of the radar/telescope.

ORDEM output in the telescope/radar mode is a cumulative flux as a function of debris size and altitude, where flux is the number of debris per unit area per unit time. Cumulative flux represents the flux of debris of a given size and larger and is defined as

$$F(h, l) = \int_{l}^{\infty} f(h, l')\, dl' \tag{A7}$$

where F is the cumulative flux, f is the flux density, h is altitude, and l is debris size. ORDEM only calculates cumulative flux in decade steps from 10 μm to 1 m. For the proceeding calculations, the flux is first interpolated from the six provided fiducial points to 1000 logarithmically spaced points using the Piecewise Cubic Hermite Interpolating Polynomial algorithm (Fritsch & Butland 1984). This algorithm was chosen because it preserves monotonicity, which is important when interpolating cumulative curves. After this, to predict a total count rate, we compute the lateral surface area as a function of altitude, $A(h)$. Additionally, the sensitivity of the radar must be taken into account by computing a probability of detection, P_D. Since it is a function of the debris size, we integrate over the product of the probability of detection and flux density to estimate sensitivity-limited cumulative flux. Flux density is recovered from cumulative flux through differentiation.

$$f(h, l) = -\frac{dF}{dl} \tag{A8}$$

Single-pulse probability of detection is calculated using the noncentral chi-squared distribution with 4 degrees of freedom depending on S/N_T, the S/N threshold used to declare a detection, and the actual S/N. S/N can be estimated using the bistatic radar equation:

$$S/N = \frac{P_t G_t G_r \lambda^2 \sigma F_t^2 F_r^2}{(4\pi)^3 k_B T_s \Delta f R_t^2 R_r^2} \tag{A9}$$

where P_t is the peak transmit power, G is the peak gain, λ is the wavelength, F is the pattern propagation factor, k_B is Boltzmann's constant, T_s is the system temperature, Δf is the receiver bandwidth, R is range to target, L is a general loss term, σ is the RCS, and the t and r subscripts indicate the transmitter and receiver, respectively. RCS is related to the debris size using the NASA-SEM, which is a function of RCS and radar wavelength. Since the SEM gives a one-to-one mapping between RCS and size, we can invert the SEM to estimate the RCS of debris of a certain size.

$$l = \mathrm{SEM}(\sigma, \lambda) \rightarrow \sigma = \mathrm{SEM}^{-1}(l, \lambda) \tag{A10}$$

Combining everything, for each ORDEM debris size, its RCS is estimated. From the RCS and transmitter/receiver characteristics, the S/N that would be measured by the radar is calculated. This S/N along with the S/N threshold used for detection declaration is used to compute the probability of detection for the debris size. The sensitivity-limited cumulative

flux is then calculated as

$$F'(h, l) = \int_l^{\infty} f(h, l')P_D(l')\,dl' = \int_l^{l_0} f(h, l')P_D(l')\,dl' + F_0(h). \quad \text{(A11)}$$

Since we cannot numerically integrate to infinity, we split the integral for F at l_0, the largest size for which ORDEM provides a cumulative flux, where $F_0(h) = \int_{l_0}^{\infty} f(h, l')P_D(l')dl' = \int_{l_0}^{\infty} f(h, l')dl'$ is the cumulative flux at the largest size for which ORDEM provides a cumulative flux and assumes probability of detection at this size to be 1. Cumulative count rate is calculated by integrating the cumulative flux/area product over the altitude.

$$\dot{N}(l) = \int_{h_0}^{h_1} A(h)F'(h, l)\,dh \quad \text{(A12)}$$

Area is calculated as described in Section A.3. Assuming that the product $f(h, l)P_D(l)$ approaches zero as l approaches zero, the total count rate, $\dot{N}_T$, is estimated by taking the limit of the cumulative count rate as l approaches zero.

$$\dot{N}_T = \lim_{l \to 0} \dot{N}(l) \quad \text{(A13)}$$

For the bistatic geometries contained herein, the calculation of debris detection rates assumes that the beam-intersection point is located at 1000 km in altitude.

ORCID iDs

James Murray https://orcid.org/0000-0002-5400-0490

References

Balogun, F. A., Brunetti, A., & Cesareo, R. 2000, RaPC, 59, 23
Barber, C. B., Dobkin, D. P., & Huhdanpaa, H. 1996, ACM Transactions on Mathematical Software, 22, 469
Beyer, W. A., Fawcett, L. R., Mauldin, R. D., & Swartz, B. K. 1987, JSymC, 4, 381
Briczinski, S. J., Mathews, J. D., & Meisel, D. D. 2009, JGRA, 114, A04311
Fritsch, F. N., & Butland, J. 1984, SIAM Journal on Scientific and Statistical Computing, 5, 300
GBT Scientific Staff 2021, Observing with the Green Bank Telescope, Green Bank Observatory, https://www.gb.nrao.edu/scienceDocs/GBTog.pdf
Hubbell, J. 1965, Journal of Research, 69C, 139
Hughes, R. G., & Clamons, J. D. 1974, Volume Intersection of Two Identical Right Circular Cones, AD-781 649, Naval Research Laboratory, https://apps.dtic.mil/sti/pdfs/AD0781649.pdf
Janches, D., Mathews, J., Meisel, D., & Zhou, Q.-H. 2000, Icar, 145, 53
Lee, C. G., Slade, M. A., Jao, J. S., & Rodriguez-Alvarez, N. 2020, Journal of Space Safety Engineering, 7, 242
Letsch, R., Leushacke, L., Rosebrock, J., et al. 2009, in Proc. of the Fifth European Conf. on Space Debris, ed. H. Lacoste (Paris: ESA), 33
Leushacke, L., Mehrholz, D., & Jehn, R. 1997, in Second European Conf. on Space Debris (Paris: ESA), 45
Levanon, N. 2009, ITAES, 45, 687
Liou, J.-C. 2020, in 2nd IAA Conf. on Space Situational Awareness (Washington, DC: NASA), https://ntrs.nasa.gov/api/citations/20200000450/downloads/20200000450.pdf
Morselli, A., Armellin, R., Di Lizia, P., et al. 2014, LVX Int. Astronautical Congress (Int. Astronautical Federation), IAC-14-A6.9.4
Muntoni, G., Schirru, L., Pisanu, T., et al. 2017, Electronics, 6, 59
Murray, J. 2019, Orbital Debris Quarterly News, 23, 8, https://orbitaldebris.jsc.nasa.gov/quarterly-news/pdfs/odqnv23i1.pdf
Murray, J., Blackwell, C., Gaynor, J., & Kennedy, T. 2019a, Haystack Ultra-Wideband Satellite Imaging Radar Measurements of the Orbital Debris Environment: 2014-2017, NASA/TP-2019-220302, https://ntrs.nasa.gov/api/citations/20190028719/downloads/20190028719.pdf
Murray, J., & Kennedy, T. 2020, Haystack Ultra-Wideband Satellite Imaging Radar Measurements of the Orbital Debris Environment: 2018, NASA/TP-2020-5006606, https://ntrs.nasa.gov/api/citations/20205006606/downloads/TP-2020-5006606_HUSIR%20CY18%20Report_final.pdf
Murray, J., Miller, R., Matney, M., Anz-Meador, P., & Kennedy, T. 2019b, LPSC, 2109, 6138
NAIC 2020, Arecibo Observatory Receivers, https://www.naic.edu/~astro/RXstatus/rcvrtabz.shtml
National Research Council 1998, Protecting the Space Shuttle from Meteoroids and Orbital Debris (Washington, DC: The National Academies Press)
Perilat, P. 2020, Patriot 12 meter telescope, https://www.naic.edu/~phil/hardware/12meter/patriot12meter.html
Pupillo, G., Bartolini, M., Cevolani, G., et al. 2008, MSAIS, 12, 44
Romney, J. 2019, Frequency Bands & Performance, NRAO, https://science.nrao.edu/facilities/vlba/docs/manuals/oss2019B/bands-perf
Roshi, D. A., Aponte, N., Araya, E., et al. 2021, The Future Of The Arecibo Observatory: The Next Generation Arecibo Telescope, White Paper, ver 2.0, http://www.naic.edu/ngat/NGAT_WhitePaper_rv9_05102021.pdf
Ruiz, G., Leushacke, L., Jehn, R., & Keller, R. 2006, in LVII Int. Astronautical Congress (Int. Astronautical Federation), IAC-06-B6.1.07
Ruiz, G., Leushacke, L., & Rosebrock, J. 2005, in Proc. of the 4th European Conf. on Space Debris, ed. D. Danesy (Paris: ESA), 89
Saba, L., Di Martino, M., Delbo, M., et al. 2005, MSAIS, 6, 104
Salter, C. 2020, An Astronomer's Guide to the Arecibo 305-m Telescope, NAIC, http://www.naic.edu/ao/scientist-user-portal/astronomy/astronomer-guide
Skolnik, M. I. 1990, Radar Handbook, Electronic Engineering Series (New York: McGraw-Hill)
Squire, M. D., Cooke, W. J., Williamsen, J., et al. 2015, Joint Polar Satellite System (JPSS) Micrometeoroid and Orbital Debris (MMOD) Assessment, NASA/TM-2015-218780, https://ntrs.nasa.gov/api/citations/20150017054/downloads/20150017054.pdf
Stansbery, E., Matney, M., Krisko, P., et al. 2014, NASA Orbital Debris Engineering Model ORDEM 3.0 - User's Guide, NASA/TP-2014-217370
Sulzer, M. P. 2004, Atmospheric Chemistry and Physics Discussions, 4, 947
Thompson, T. W., Goldstein, R. M., Campbell, D. B., Stansbery, E. G., & Potter, A. E. 1992, GeoRL, 19, 257
Virtanen, P., Gommers, R., Oliphant, T. E., et al. 2020, NatMe, 17, 261
Wen, C. -H., Doherty, J. F., & Mathews, J. D. 2004, ITGRS, 42, 501
Wen, C. -H., Doherty, J., & Mathews, J. 2005a, JASTP, 67, 1190
Wen, C. -H., Doherty, J. F., Mathews, J. D., & Janches, D. 2005b, JASTP, 67, 275
Xu, Y. -I., Stokely, C., Matney, M., & Stansbery, E. 2005, in LVI Int. Astronautical Congress (Int. Astronautical Federation), IAC-05-B6.1.02
Zaitsev, A. L., Ignatov, S. P., di Martino, M., Montebugnoli, S., & Nabatov, A. S. 2001, in Proc. of the Third European Conf. on Space Debris, ed. H. Lacoste (Noordwijk: ESA), 79
Zhou, Q., Tepley, C. A., & Sulzer, M. P. 1995, JATP, 57, 421
Zhou, Q. H., & Kelley, M. C. 1997, JASTP, 59, 739